Investigation of the shape of the imaginary part of the optical-model potential for electron scattering by rare gases

Grażyna Staszewska,* David W. Schwenke, and Donald G. Truhlar

Department of Chemistry, University of Minnesota, Minneapolis, Minnesota 55455

(Received 13 January 1984)

We present a comparative study of several empirical and nonempirical models for the absorption potential, which is the imaginary part of an optical-model potential, for electron scattering by rare gases. We show that the elastic differential cross section is most sensitive to the absorption potential for high-impact energy and large scattering angles. We compare differential cross sections calculated by several models for the absorption potential and by several arbitrary modifications of these model potentials. We are able to associate the effect of the absorption potential on the elastic differential cross section with its form at small electron-atom distances r, and we are able to deduce various qualitative features that the absorption potential must possess at small and large r in order to predict both accurate differential cross sections and accurate absorption cross sections. Based on these observations, the Pauli blocking conditions of the quasifree scattering model for the absorption potential are modified empirically, thus producing a more accurate model that may be applied to other systems; e.g., electron-molecule scattering, with no adjustable parameters.

I. INTRODUCTION

In this paper we are concerned with optical-model potentials for electron scattering by atoms. By an optical-model potential we shall mean a local, energy-dependent potential that yields an approximation to the correct scattering matrix in the elastic channel. Above the first threshold energy such a potential should be complex, and the imaginary part is called the absorption potential. There are several approaches to calculating the absorption potential. These include *empirical* and *nonempirical* methods. In empirical methods, a functional form containing parameters is postulated, and one or more parameters are adjusted to experiment, usually to the absorption cross section (which is the sum of the all electronically inelastic and ionization cross sections) and/or the elastic differential cross section.[1-5] The nonempirical approaches include the eikonal optical model,[6-11] the dispersion-relation method,[4,12] and a quasifree scattering, binary-collision model.[13-15] Although both the empirical and nonempirical approaches have had some successes there has been little *direct* comparison of these methods, and it is not understood which features of the absorption potentials are crucial to their successes, and which are less critical. The present paper makes a direct comparison of the available models as well as some *ad hoc* and semiempirical variations of the absorption potentials. The goal of the comparisons is to elucidate the magnitude and shape of the absorption potential at various ranges of electron-atom distance.

As a consequence of these comparisons, we are able to modify the Pauli-blocking conditions of the quasifree scattering model to produce a more successful version. Since the modified Pauli-blocking conditions are arrived at empirically, rather than derived, the new version is partly empirical. We shall call it a *semiempirical* model

to differentiate it from the previously available empirical models. The previous empirical models required several parameters to be adjusted for a given target[3] or one parameter to be adjusted for each combination of target and impact energy.[1,2] The new semiempirical method may be applied to new targets and new impact energies with no further adjustment. Thus it is easier to use, and it has more value for predictive purposes, rather than just for correlation, interpolation, and interpretation of a preexisting data base.

Section II presents a few results to illustrate the general effect of the absorption potential, and Sec. III presents a detailed study of electron-neon scattering at 400- and 50-eV impact energies. This illustrates the effect of various features of the absorption potential on calculated cross sections. Section III also presents two new semiempirical models, the most successful of which is called the quasifree-scattering model, version 3. Section IV presents a systematic test of the quasifree-scattering model, version 3, against experimental results[16-27] for electron scattering by helium, neon, and argon at 30–1000-eV impact energies. Section V summarizes the most important conclusions.

It is convenient to use a systematic set of abbreviations for the various potentials. These are summarized in alphabetical order in Appendix A. Except for the absorption potentials, the methods employed in the present calculations are the same as described elsewhere in conjunction with other recent optical-model-potential studies[4,5,12-15,28-30] of electron scattering by rare gases; the important details are specified in Appendix B.

We express all potentials in hartree atomic units in which the energy unit is the hartree ($1E_h = 27.212$ eV $= 4.3598 \times 10^{-18}$ J), the length unit is the bohr ($1a_0 = 0.529\,18 \times 10^{-10}$ m), and $\hbar$ and the mass of an electron are unity.

II. EFFECT OF ABSORPTION

The empirically most successful absorption potential proposed so far is that of McCarthy, Noble, and co-workers;[2] in particular, when the parameter of this model is adjusted at each energy so that the calculated absorption cross section agrees with experiment, it yields differential cross sections in good agreement with recent measurements for both small and large angles over a wide range of energy for several rare-gas targets. Figure 1 compares this potential for electron-neon scattering at 50- and 400-eV impact energies to the real part of the optical-model potential. We take the real part to be the sum of static,[31] exchange,[32] and polarization[33] terms, and we present results for two different models for the polarization, an energy-independent adiabatic approximation, and an energy-dependent nonadiabatic one. Further details of the real parts of the optical-model potentials are provided in Appendix B. Cross sections computed using these potentials are shown in Table I. (The abbreviations used in figures and column headings of tables are summarized in Appendix A, and the notation used for cross sections in Table I and elsewhere in this paper is defined in Appendix B.) Table I also shows cross sections calculated neglecting the absorption potential (as explained in Appendix A, the model without absorption is called model SEPa because it includes the static, exchange, and adiabatic polarization potentials). The main conclusions to be drawn from Table I are as follows: For both energies the inclusion of an absorption potential lowers the elastic differential cross section for larger scattering angles, greater than 42 deg for 50 eV and greater than 16 deg for 400 eV. The amount of this lowering is about the same for both energies and is as much as a factor of 1.5. For small angles, the absorption potential of McCarthy, Noble, and co-workers increases the differential cross section by as much as a factor of 1.1. The choice between the two po-
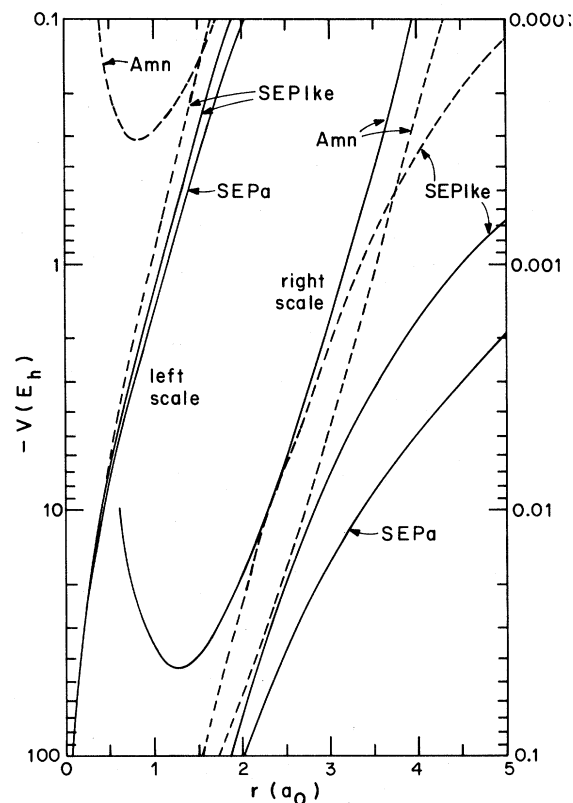

FIG. 1. Real and imaginary parts of optical-model potentials for electron-neon scattering at impact energies of 50 and 400 eV. The abbreviations are explained in Appendixes A and B. Solid curves are for 50 eV, and dashed curves are for 400 eV.

larization potentials effects the cross sections mainly at small scattering angles and has a negligible effect on the absorption cross sections. Thus, even though we are unsure of the correct form of the polarization term in the

TABLE I. Cross sections for electron-neon scattering at two impact energies as calculated by various models.

Energy (eV)	50	50	50	400	400	400
Model	SEPa	SEPaAmn	SEPlkeAmn	SEPa	SEPaAmn	SEPlkeAmn
c (a.u.)[a]		0.630	0.632		107.7	106.0
$\sigma_{el}(a_0^2)$	11.36	10.65	10.67	4.31	3.85	3.01
$\sigma_{el}^m(a_0^2)$	9.87	8.64	8.27	1.22	0.93	0.87
$\sigma_{abs}(a_0^2)$	0	1.85	1.85	0	2.30	2.30
$\sigma_{tot}(a_0^2)$	11.36	12.50	12.52	4.31	6.15	5.31

θ (deg)	$\dfrac{d\sigma}{d\Omega}$ (a_0^2/sr)					
0	6.43	7.04	4.45	15.26	17.32	8.39
15	3.76	4.06	3.51	4.14	4.17	3.23
30	1.86	1.99	2.26	0.910	0.644	0.564
60	0.851	0.746	0.854	0.154	0.110	0.093
90	0.261	0.206	0.131	0.083	0.062	0.055
105	0.031	0.022	0.019	0.073	0.056	0.052
120	0.205	0.190	0.238	0.069	0.053	0.053
150	1.83	1.59	1.45	0.067	0.053	0.057
180	3.00	2.58	2.22	0.066	0.054	0.059

[a]The parameter c defined in Sec. III by Eq. (17).

real part of the optical-model potential, in the present paper we study and empirically refine the absorption potential by concentrating only on the large-angle scattering and the absorption cross section. An important point learned from preceding works[13-15] is that the original quasifree-scattering model predicts reasonably accurate absorption cross sections at both intermediate and high energies and reasonably accurate differential cross sections at intermediate energies, but it seriously underestimates the large-angle scattering at high energy.

III. COMPARISON OF
ABSORPTION-POTENTIAL MODELS

The models to be applied most widely in the present paper are those based on the quasifree-scattering model with Pauli blocking and those based on the model of McCarthy and co-workers. In the quasifree-scattering model[13-15] the absorption potential for impact energy E at a point $\vec{r}$ is

$$V^A(\vec{r},E) = -\tfrac{1}{2}v_{\text{loc}}\rho\bar{\sigma}_b , \qquad (1)$$

where

$$v_{\text{loc}}(\vec{r},E) = [2(E - V^{\text{SE}})]^{1/2} . \qquad (2)$$

In Eqs. (1) and (2), $v_{\text{loc}}(\vec{r},E)$ is the local speed of an incident electron, $V^{\text{SE}}(\vec{r},E)$ is the static-plus-exchange potential, $\rho(\vec{r})$ is the target electron density per unit volume, and $\bar{\sigma}_b(\vec{r},E)$ is the average binary-collision cross section for Pauli-allowed electron-electron collisions. The latter quantity is obtained by averaging the Rutherford cross section (with a semiclassical correction factor of $\tfrac{1}{2}$ that approximately accounts for the effect of exchange) over a free-electron gas of density $\rho(\vec{r})$ subject to the constraints

$$(k')^2 \geq \alpha , \qquad (3)$$

$$(p')^2 \geq \beta , \qquad (4)$$

where k' and p' are the final momenta of the bound and scattering electrons, respectively, in the barycentric coordinate system. This yields

$$\bar{\sigma}_b(\vec{r},E) = \begin{cases} \dfrac{32\pi^2 N_k}{15p^2}(f_1+f_2) , & p^2 \geq \alpha+\beta-k_F^2 \\ 0 , & p^2 < \alpha+\beta-k_F^2 \end{cases} \qquad (5)$$

where

$$N_k(\vec{r}) = 3/(4\pi k_F^3) , \qquad (6)$$

$$p(E) = (2E)^{1/2} , \qquad (7)$$

$$f_1(\vec{r},E) = \frac{5k_F^3}{(\alpha-k_F^2)} - \frac{k_F^3[5(p^2-\beta)+2k_F^2]}{(p^2-\beta)^2} , \qquad (8)$$

$$f_2(\vec{r},E) = \begin{cases} 0 , & p^2 > \alpha+\beta \\ \dfrac{2(\alpha+\beta-p^2)^{5/2}}{(p^2-\beta)^2} , & p^2 \leq \alpha+\beta \end{cases} \qquad (9)$$

$$k_F(\vec{r}) = (3\pi^2\rho)^{1/3} . \qquad (10)$$

In Eqs. (5)–(10), $p(E)$ is the incident momentum of the scattering electron and $k_F(\vec{r})$ is the target Fermi momentum. Since $V^A(\vec{r},E)$ must be zero below the threshold energy Δ and nonzero above it, Eqs. (1), (5), and (7) imply that

$$\min_{\{\vec{r}\}}[\alpha(\vec{r},E)+\beta(\vec{r},E)-k_F^2(\vec{r})] = 2\Delta . \qquad (11)$$

In the original quasifree-scattering model we used a simple model of an electron interacting with a free-electron gas to obtain

$$\alpha(\vec{r},E) = k_F^2+2\Delta \qquad (12)$$

and

$$\beta(\vec{r},E) = k_F^2 . \qquad (13)$$

In a free-electron gas all energy is kinetic, and the interpretation of Eqs. (3) and (12) is that the lowest-energy state available to the initially bound electron exceeds the Fermi level by the energy gap Δ. Similarly the interpretation of Eqs. (4) and (13) is that the initially unbound electron is not allowed to fall into the occupied Fermi sea. Note that Eqs. (12) and (13) are consistent with Eq. (11) because

$$\min_{\{\vec{r}\}} k_F(\vec{r}) = k_F(r=\infty) = 0 . \qquad (14)$$

Clearly Eqs. (12) and (13) result from a very simple model; the difficulty with improving on them is that the free-electron-gas model is incompatible with most models involving orbital energies or realistic local kinetic energies, and hence it is hard to incorporate the true structure of the target into the Pauli-blocking conditions.

One way around this impass is to simplify the model and introduce an empirical parameter. Although the models of McCarthy and co-workers[1,2] preceded the quasifree-scattering model, we think it is instructive to discuss them as if they are simplified versions of it. The original version of the models of McCarthy and co-workers is the model of Furness and McCarthy.[1] They set

$$V^A(\vec{r},E) = c\rho T_{\text{loc}}^{-2} , \qquad (15)$$

where $c(E)$ is an empirical constant and $T_{\text{loc}}(\vec{r},E)$ is the local kinetic energy. For our calculations we approximate the latter by

$$T_{\text{loc}}(\vec{r},E) = E - V^{\text{SEPa}} , \qquad (16)$$

where $V^{\text{SEPa}}(\vec{r},E)$ is the real part of the optical-model potential. The factor $[T_{\text{loc}}(\vec{r},E)]^{-2}$ gives the energy dependence of the Rutherford cross section without Pauli blocking so Eq. (15) may be considered to be proportional to Eq. (1) with the local speed factor neglected and the Pauli blocking not explicitly included. [If Pauli blocking is really neglected in Eq. (1), the right side becomes infinite.] In a later paper McCarthy, Noble, and co-workers replaced Eq. (15) by

$$V^A(\vec{r},e) = cr^2\rho_H T_{\text{loc}}^{-2} , \qquad (17)$$

where r is the distance from the center of mass of the target, $\rho_H(\vec{r})$ is the density of the highest occupied orbital,

and $c(E)$ is a new empirical constant. [We will call all the empirical constants $c(E)$ although of course they have different values in the different models.] The replacement of $\rho(\vec{r})$ by $\rho_H(\vec{r})$ could be approximately justified in the context of the quasifree-scattering model as a severe form of Pauli blocking, i.e., the electrons in more tightly bound orbitals have a larger fraction of their final phase space Pauli blocked. Nevertheless this replacement and the multiplication by r^2 can only be justified empirically.

In light of the above discussion it seems natural to try to combine the physics of the full quasifree-scattering model with the empirical approach by introducing the empiricism at a different stage. In particular we suggest that one retain Eqs. (1)—(4) but treat $\alpha(\vec{r},E)$ and $\beta(\vec{r},E)$ as arbitrary functions subject only to the constraint of Eq. (11). We will actually enforce another restriction on these functions, namely that the functional forms, like Eqs. (12) and (13), be monotonically decreasing functions of r for electron-atom scattering. This enforces the physically reasonable condition that Pauli blocking should be more severe for electrons nearer to the nuclei since these electrons are lower in the Fermi sea.

We note here that the model of McCarthy, Noble, and co-workers and the model of Green *et al.* are empirically the most successful optical-model potentials that have been applied so far. Figure 2 compares these potentials for electron-neon scattering at 400 eV to the original version of the potential of McCarthy and co-workers and to the potential of the original quasifree-scattering model. To see the effect of differences in the absorption potentials on the scattering cross sections we present a comparison of calculated cross sections for these potentials in Table II. (The other results in Fig. 2 and Table II are explained below.) In order that the calculated cross sections in Table II (as well as Tables III and IV discussed below) should reflect only the differences in the absorption potential, they are all based on the same real part for the optical-model potential; in particular they are based on the real part called SEPa in Sec. II and Appendix A. (As discussed in Sec. II, the choice of real part should not have a great effect on our conclusions.)

Figure 2 shows that the original quasifree scattering model predicts a much deeper and shorter-range absorption potential than either of the two successful empirical models. Table II shows that the original quasifree-scattering model predicts too small a cross section at large scattering angles.

In order to learn what range of r is most important for governing the differences in the predicted cross sections we also examined several additional models. The next model considered is a (new) third version of a potential of the type used by McCarthy and co-workers. We define this by

$$V^A(\vec{r},E) = c\rho_H T_{\text{loc}}^{-2} , \tag{18}$$

where $c(E)$ is a new empirical scale factor. (In every case c is chosen to make the absorption cross section agree with experiment.) Equation (18) yields an absorption potential similar to Eq. (15) at large r but relatively more like Eq. (17) at small r; the scattering results, however, are very similar to these for Eq. (15). This illustrates the im-
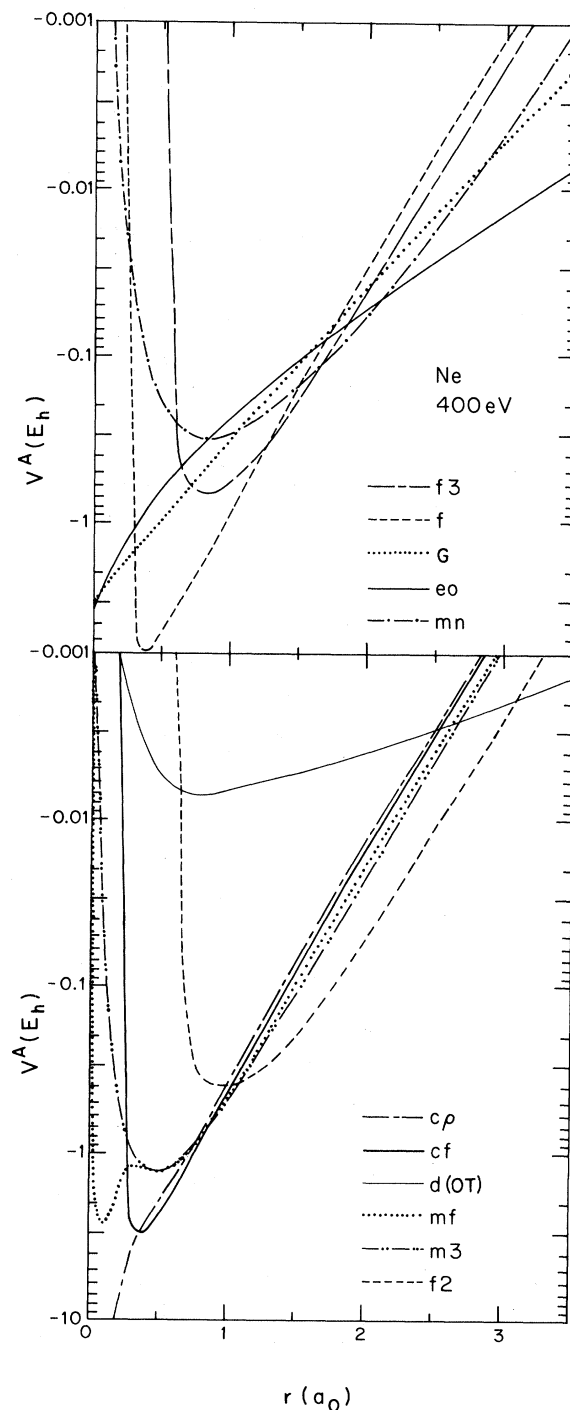

FIG. 2. Various empirical and nonempirical absorption potentials for electron-neon scattering at impact energy 400 eV: f, original quasifree-scattering model (Refs. 13—15); cf, quasifree-scattering model with empirical scale factor; f2,f3, quasifree-scattering model with modified Pauli-blocking conditions; eo, eikonal optical model; d(OT), dispersion-relation absorption potential based on Onda-Truhlar energy-dependent polarization potential; mn, mf, m3, three versions of the model of McCarthy and co-workers; G, model of Green *et al.*; cρ, empirical scale factor times the density. See the text and Appendix A for more complete descriptions of the various models.

TABLE II. Results for electron-Ne scattering at 400 eV. Theoretical results are for various SEPaA models.

	expt.[a]	expt.[b]	f	g	mf	mn	m3	cρ	d(OT)	eo	cf	f2	f3
c (a.u.)					269.9	107.7	175.64	0.86708			0.535		
$\sigma_{el}(a_0^2)$	3.22	3.24	2.65	3.38	3.23	3.85	3.32	2.79	3.29	3.57	3.02	3.89	3.71
$\sigma_{el}^m(a_0^2)$		0.88	0.26	0.65	0.57	0.93	0.64	0.25	1.13	0.75	0.49	0.93	0.82
$\sigma_{abs}(a_0^2)$	2.30		3.50	2.43	2.30	2.30	2.30	2.30	0.66	3.34	2.32	2.42	2.57
$\sigma_{tot}(a_0^2)$	5.51		6.15	5.81	5.53	6.15	5.62	5.09	3.95	6.92	5.34	6.31	6.28
θ (deg)						$d\sigma/d\Omega$ (a_0^2/sr)							
3	8.21		11.30	13.17	12.06	14.25	12.24	11.55	6.19	15.24	11.28	14.49	13.90
5	4.97	5.39	9.66	11.06	10.27	12.13	10.43	9.76	5.63	12.33	9.57	12.40	11.92
10	1.84	1.96	6.23	6.76	6.55	7.47	6.65	6.15	4.30	6.85	6.09	7.78	7.59
20			1.99	2.08	2.19	2.20	2.20	2.06	1.96	2.05	2.09	2.28	2.33
30	0.693	0.729	0.491	0.625	0.622	0.644	0.630	0.590	0.780	0.655	0.636	0.589	0.584
40	0.301	0.340	0.118	0.236	0.197	0.266	0.209	0.173	0.346	0.263	0.210	0.230	0.191
50	0.166	0.169	0.040	0.125	0.095	0.156	0.103	0.067	0.192	0.144	0.091	0.149	0.114
60	0.103		0.021	0.084	0.066	0.110	0.069	0.034	0.129	0.098	0.053	0.112	0.090
70	0.082		0.014	0.063	0.051	0.086	0.053	0.024	0.099	0.074	0.037	0.088	0.074
80	0.067		0.011	0.050	0.041	0.071	0.043	0.016	0.083	0.059	0.029	0.072	0.062
90	0.057		0.0091	0.042	0.035	0.062	0.037	0.011	0.074	0.050	0.025	0.063	0.054
100	0.051		0.0086	0.037	0.031	0.057	0.035	0.0070	0.070	0.045	0.023	0.059	0.050
110	0.050		0.0088	0.034	0.029	0.054	0.033	0.0048	0.068	0.041	0.023	0.056	0.048
120	0.048		0.0094	0.033	0.028	0.053	0.034	0.0036	0.068	0.039	0.023	0.055	0.048
130	0.047		0.010	0.032	0.028	0.053	0.034	0.0030	0.069	0.038	0.024	0.054	0.048
140	0.047		0.011	0.031	0.029	0.053	0.035	0.0029	0.070	0.037	0.025	0.053	0.049
150	0.046		0.012	0.030	0.029	0.053	0.036	0.0030	0.072	0.036	0.026	0.053	0.050
160			0.012	0.030	0.030	0.054	0.037	0.0031	0.073	0.036	0.026	0.052	0.051
170			0.013	0.030	0.030	0.054	0.037	0.0033	0.073	0.036	0.027	0.052	0.051
l				Partial-wave contributions to absorption cross section (a_0^2)									
0			0.089	0.051	0.055	0.023	0.048	0.106	0.001	0.043	0.066	0.024	0.031
1–5			2.433	1.282	1.586	0.965	1.533	1.708	0.047	1.072	1.709	1.066	1.385
6–10			0.874	0.772	0.586	1.005	0.640	0.434	0.088	0.954	0.486	1.125	1.006
11–15			0.096	0.240	0.066	0.267	0.073	0.046	0.089	0.560	0.052	0.188	0.136
16–20			0.009	0.063	0.006	0.036	0.005	0.004	0.074	0.306	0.005	0.019	0.014
21–25			0.001	0.016	0.0006	0.003	0.0003	4.17(−4)[c]	0.059	0.170	4.7(−4)	0.002	0.001
26–∞			9.55(−5)	4.8(−3)	5.32(−5)	1.20(−5)	2.66(−4)	5.40(−5)	0.299	0.236	5.5(−5)	1.98(−4)	1.35(−4)

[a]References 17 and 26.

[b]Reference 23.

[c]Number in parentheses is powers of ten.

TABLE III. Cross sections for electron-Ne scattering at 400 eV in SEPaAeo and SEPaAeoj models.

	eo	eo1	eo2	eo3	eo4	eo5	eo6	eo7	eo8
$\sigma_{el}(a_0^2)$	3.57	3.60	3.59	3.58	3.58	3.62	3.88	3.57	3.57
$\sigma_{el}^m(a_0^2)$	0.75	0.79	0.77	0.77	0.76	0.80	0.95	0.75	0.75
$\sigma_{abs}(a_0^2)$	3.34	1.35	1.66	1.98	2.19	3.31	3.12	2.61	3.08
$\sigma_{tot}(a_0^2)$	6.92	4.95	5.25	5.56	5.77	6.93	7.00	6.18	6.65

θ (deg)					$d\sigma/d\Omega(a_0^2)$				
3	15.24	12.28	12.68	13.16	13.50	15.26	15.67	14.21	15.00
5	12.33	10.41	10.77	11.17	11.43	12.34	12.71	11.96	12.35
10	6.85	6.63	6.82	6.94	6.98	6.87	7.13	7.04	6.86
20	2.05	2.31	2.23	2.14	2.10	2.06	2.17	2.03	2.05
30	0.655	0.699	0.656	0.653	0.656	0.664	0.705	0.667	0.657
40	0.263	0.259	0.265	0.269	0.268	0.270	0.285	0.262	0.264
50	0.144	0.150	0.151	0.148	0.147	0.148	0.158	0.146	0.144
60	0.098	0.103	0.101	0.100	0.100	0.100	0.112	0.099	0.098
70	0.074	0.077	0.077	0.075	0.075	0.075	0.088	0.074	0.074
80	0.059	0.063	0.061	0.060	0.060	0.061	0.073	0.060	0.059
90	0.050	0.054	0.051	0.051	0.051	0.052	0.064	0.050	0.050
100	0.045	0.047	0.046	0.045	0.045	0.047	0.058	0.045	0.045
110	0.041	0.042	0.042	0.042	0.042	0.045	0.055	0.042	0.041
120	0.039	0.040	0.040	0.040	0.040	0.043	0.054	0.039	0.039
130	0.038	0.039	0.039	0.039	0.038	0.042	0.054	0.038	0.038
140	0.037	0.039	0.038	0.038	0.038	0.042	0.055	0.037	0.037
150	0.036	0.039	0.037	0.037	0.037	0.041	0.056	0.037	0.036
160	0.036	0.038	0.037	0.037	0.037	0.041	0.057	0.036	0.036
170	0.036	0.038	0.037	0.037	0.036	0.041	0.058	0.036	0.036

l					partial-wave contributions to $\sigma_{abs}(a_0^2)$				
0	0.043	0.040	0.041	0.042	0.042	0.035	0.020	0.043	0.043
1—5	1.072	0.940	0.987	1.018	1.033	1.048	0.870	1.058	1.070
6—10	0.954	0.367	0.599	0.747	0.808	0.954	0.954	0.909	0.947
11—15	0.560	0.001	0.036	0.167	0.267	0.560	0.560	0.476	0.547
16—20	0.306	4.0(−8)	1.1(−4)	0.010	0.040	0.306	0.306	0.118	0.287
21—25	0.170	0	3.8(−8)	1.8(−4)	0.003	0.170	0.170	0.001	0.142
26—∞	0.236	0	0	1.0(−6)	1.2(−4)	0.236	0.236	0	0.046

portance of the large-r behavior of the absorption potential and of the factor of r^2 in Eq. (17).

An even simpler empirical model along the lines of the quasifree-scattering model is

$$V^A(\vec{r},E)=c\rho , \tag{19}$$

where $c(E)$ is now another empirical scale factor. Equation (19) is even more simplified (and basic) than Eq. (15); it simply makes the absorption potential proportional to the density of electrons. Figure 2 shows that this leads to an even shorter-range absorption potential than the original quasifree-scattering model and one that is deeper for $r \lesssim 0.3a_0$. Table II shows that the potential of Eq. (19) predicts a smaller absorption cross section than the original quasifree model but an even smaller large-angle cross section, i.e., less absorption overall but more absorption of flux that would otherwise exit at large scattering angles. Apparently the refinements of the original quasifree-scattering model as compared to Eq. (19) do modify the shape of the absorption potential in the correct direction, but they do not go far enough.

Figure 2 and Table II also include two more nonempirical models. First consider the absorption potential ob-

tained[4,12] by applying the dispersion relation[34] relating the imaginary and real parts of an optical-model potential to the real part obtained by the energy-dependent polarization potential of Onda and Truhlar.[35] That polarization potential, and hence the resulting absorption potential, is expected to be most valid at low energy, but it is presented because it makes such an interesting comparison: it is much weaker than the other model absorption potentials at small r but it is approximately equal to the absorption potential of McCarthy, Noble, and co-workers at $R \cong 3.4a_0$. Table II shows, however, that the absorption cross section predicted by this dispersion-relation potential is much too small. This indicates that the important region for absorption is primarily at distances less than $3.4a_0$. The final nonempirical model to be discussed is the eikonal optical model. This is stronger than the absorption potential of McCarthy, Noble, and co-workers both for $r \lesssim 0.8a_0$ and $r \gtrsim 2.1a_0$. It does lead to a significantly larger absorption cross section but only slightly more absorption at large scattering angles. Comparing the optical-eikonal-model potential to that of Green et al. seems to indicate that its major deficiency is associated with large r, but the deep potential at very small r may account for an excess of absorption at very large scatter-

STASZEWSKA, SCHWENKE, AND TRUHLAR

TABLE IV. Cross sections for electron-Ne scattering at 400 eV in SEPaA$c\rho$ and SEPaA$c\rho j$ models.

	$c\rho$	$c\rho 1$	$c\rho 2$	$c\rho 3$
$\sigma_{el}(a_0^2)$	2.79	2.91	4.00	3.21
$\sigma_{el}^m(a_0^2)$	0.25	0.43	1.03	0.47
$\sigma_{abs}(a_0^2)$	2.30	2.20	1.23	1.96
$\sigma_{tot}(a_0^2)$	5.09	5.10	5.23	5.18
θ (deg)		$d\sigma/d\Omega$ (a_0^2/sr)		
3	11.55	11.23	13.05	12.08
5	9.76	9.49	11.10	10.24
10	6.15	5.97	7.10	6.51
20	2.06	2.00	2.46	2.23
30	0.590	0.589	0.756	0.673
40	0.173	0.192	0.277	0.225
50	0.067	0.090	0.160	0.106
60	0.034	0.058	0.122	0.067
70	0.024	0.042	0.097	0.047
80	0.016	0.032	0.079	0.035
90	0.011	0.026	0.068	0.027
100	0.0070	0.022	0.064	0.022
110	0.0048	0.019	0.062	0.019
120	0.0036	0.017	0.062	0.017
130	0.0030	0.016	0.061	0.017
140	0.0029	0.015	0.060	0.017
150	0.0030	0.015	0.058	0.017
160	0.0031	0.015	0.057	0.017
170	0.0033	0.014	0.056	0.018
l				
0	0.106	0.068	0.017	0.094
1—5	1.708	1.643	0.729	1.390
6—10	0.434	0.434	0.434	0.434
11—15	0.046	0.046	0.046	0.046
16—20	0.004	0.004	0.004	0.004
21—25	4.17(−4)	4.17(−4)	4.17(−4)	4.17(−4)
26—∞	5.40(−5)	5.40(−5)	5.40(−5)	5.40(−5)

FIG. 3. Eikonal-optical-model absorption potential with various modifications.

then loading all the rest of the absorption at large r.

We now return to the three as yet unexplained calculations in Fig. 2 and Table II. One calculation is based on applying an empirical scale factor to the original quasifree-scattering model, i.e.,

$$V^A(\vec{r},E) = -\frac{c}{2}v_{loc}\rho\bar{\sigma}_b \qquad (20)$$

with $\alpha(\vec{r},E)$ and $\beta(\vec{r},E)$ given by Eqs. (12) and (13). The result is not surprising in light of what we have learned from the arbitrary variations just discussed. The scale factor turns out to be 0.535 and this has a large effect on the deep small-r potential. Hence the effect on the large-angle scattering is big, over a factor of $2\frac{1}{2}$ at some angles.

ing angles.

Figure 3 and Table III show an attempt to make the above analysis more definitive. We started with the eikonal-optical-absorption potential and made several totally arbitrary adjustments keeping the real part of the optical-model potential fixed. For example, modification 7 shows that about 22% of the absorption in the eikonal optical model is due to $r \geq 3.6a_0$. Figure 4 and Table IV show additional variations, this time based on the absorption potential of Eq. (19). These tables show quantitatively how absorption at small r decreases the large-angle scattering. More surprising, though, is the effect of large-r absorption. This can either decrease or increase the small-angle scattering. Furthermore, a large-r change in the absorption potential may produce a very large change in the absorption cross section with only a relatively small effect on the differential cross section, whereas small-r changes in the absorption potential can produce much larger effects on the differential cross section than on the absorption cross section. This suggests that, to low order, an empirically successful optical-model potential can be constructed by putting enough absorption at small r to cause the correct decrease in large-angle scattering, and
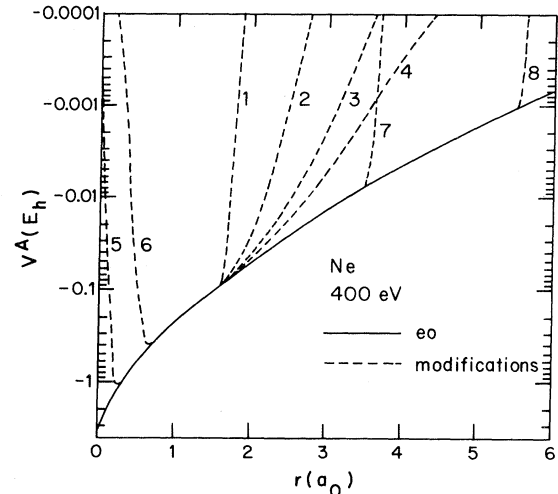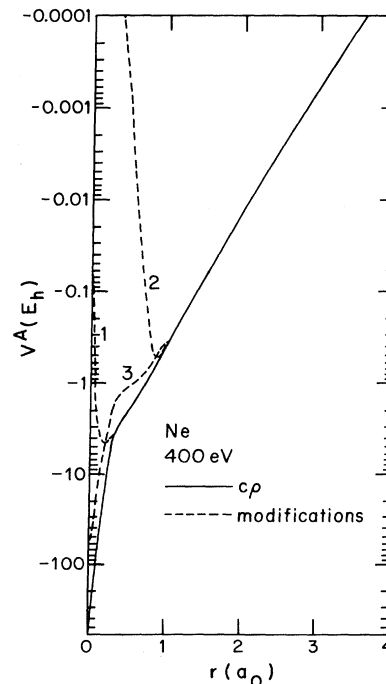

FIG. 4. Same as Fig. 3, except for absorption potential that is an empirical constant times the density.

The effect is in the correct direction but not far enough to yield good agreement with experiment. We conclude that the shape of the original quasifree-scattering absorption potential is too deep at small r and not deep enough at large r. We choose to modify $\alpha(\vec{r},E)$ and $\beta(\vec{r},E)$ semiempirically to accomplish this. We tried dozens of variations for all three rare gases at various energies, but we present results only for two of the most successful, which we will call the quasifree-scattering model, versions 2 and 3. Version 2 is based on

$$\alpha(\vec{r},E)=k_F^2+\Delta-2V^{SE} ,\qquad(21a)$$

$$\beta(\vec{r},E)=\alpha ,\qquad(21b)$$

and version 3 is based on

$$\alpha(\vec{r},E)=k_F^2+2[\Delta-(I-\Delta)]-V^{SE} ,\qquad(22a)$$

$$\beta(\vec{r},E)=k_F^2+2(I-\Delta)-V^{SE} ,\qquad(22b)$$

where I is the ionization potential. Note that $\alpha(\vec{r},E)$ and $\beta(\vec{r},E)$ are independent of energy in the original nonempirical model but we have introduced an energy dependence in the semiempirical versions, although this energy dependence is due only to exchange and is small. More important from a physical and numerical standpoint is the explicit dependence on $V^{SE}(\vec{r},E)$, which represents the local increase in kinetic energy of the incident electron as caused by the static-exchange field of the target. Table II shows that the semiempirical versions provide great improvement over the original version.

Tables II—IV also show the partial-wave contributions to the absorption cross sections, defined by

$$\sigma_{abs}=\sum_l \sigma_{abs,l} ,\qquad(23)$$

where l is the orbital angular momentum quantum number. Clearly the dispersion-relation absorption potential based on the Onda-Truhlar energy-dependent polarization potential has the longest-range contributions to absorption. In fact it was necessary to use $l_{max}=230$ to converge these calculations. The new versions of the quasifree-scattering model have larger $\sigma_{abs,l}$ at high l than the original quasifree-scattering model does, but these contributions are still smaller than those in the empirically successful models of Green et al. and McCarthy, Noble, and co-workers. It would be interesting to have high-energy coupled-channels calculations to check the $\sigma_{abs,l}$ values in these tables; this would give further insight into validity or sources of error in the various models.

So far we have explicitly discussed only 400 eV. Figure 5 and Table V are like Fig. 2 and Table II except for 50 eV. At 50 eV all three versions of the quasifree-scattering model give absorption potentials that peak between $r=1\frac{1}{2}$ and $2a_0$, whereas the McCarthy-type absorption potentials peak at r smaller than $1\frac{1}{2}a_0$. Table V shows that the differential cross sections are very similar for a wide range of shapes of absorption potential; in particular the differential cross section is less sensitive to the shape of the absorption potential at 50 eV than at 400 eV. Note also that at 50 eV the differential cross sections are more similar than the partial-wave contributions to the absorption
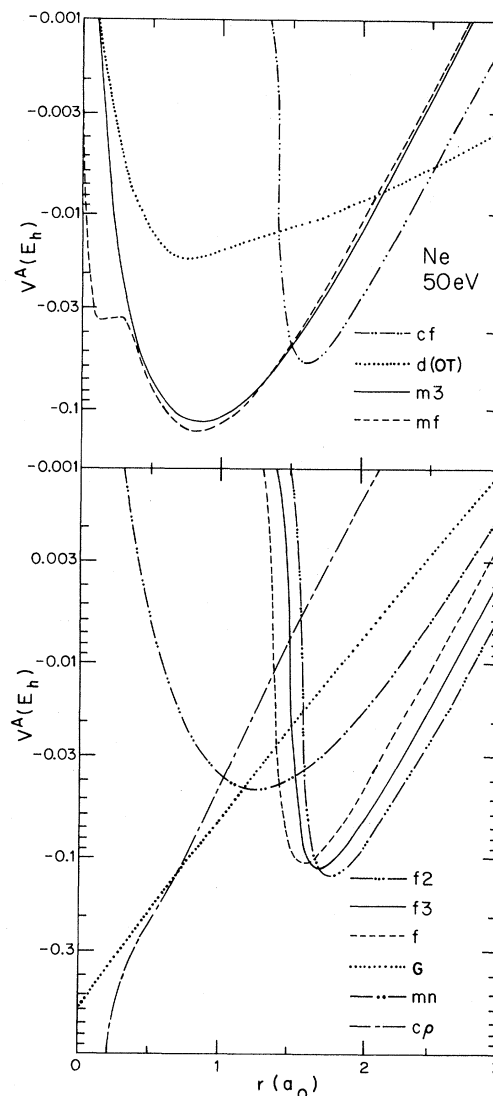

FIG. 5. Same as Fig. 2, except for 50 eV.

cross sections. One possible explanation of these trends is that at this energy the differential cross section never gets as small as it does at 400 eV. Another contributing factor is that each model yields a weaker absorption potential at 50 eV than at 400 eV. Since the mn absorption potential, which is, on the whole, the empirically most successful one for the whole 40—1000-eV range of energies considered in this paper, has about the same effect on the differential cross section at 50 eV as at 400 eV, we tentatively attribute the greater sensitivity of the differential cross sections at 400 eV to inaccuracies in some of the absorption potential shapes at the higher energy.

Note that although the differential cross sections are very insensitive to the choice of absorption potentials at 50 eV, at least for all models in Table V except the d(OT) one for small angles and the cp one for 110°—120°, the absorption cross sections are not. It is interesting to notice that the maximum absolute values of the f, f2, and f3 potentials are very similar but that the positions of these maxima shift out in the order f, f3, f2; the positions of the maxima, the strengths of these potentials at large r, and

TABLE V. Results for electron-Ne scattering at 50 eV. Theoretical results are for various SEPaA models.

c (a.u.)	mn	m3	mf	G	f	cf	f2	f3	cρ	d(OT)	expt.[a]	expt.[b]	expt.[c]	expt.[d]
c (a.u.)	0.63	1.53	2.492			0.553			0.09513					
σ_{el}	10.65	10.45	10.43	10.36	10.26	10.70	10.26	10.26	9.62	10.83	10.82			11.2
σ_{el}^m	8.64	8.33	8.31	8.08	7.85	8.68	7.67	7.77	7.32	8.71				8.57
σ_{abs}	1.85	1.85	1.85	1.84	3.21	1.85	4.41	3.75	1.85	2.34	1.85			>1.99
σ_{tot}	12.50	12.30	12.28	12.20	13.47	12.55	14.67	14.01	11.47	13.17	12.7			
θ (deg)						$d\sigma/d\Omega$ (a_0^2/sr)								
3	6.51	6.35	6.35	6.58	6.92	6.60	7.63	7.26	6.47	4.73				
5	6.06	5.91	5.90	6.12	6.55	6.14	7.16	6.80	5.99	4.44				
10	5.01	4.89	4.88	5.04	5.42	5.08	6.01	5.69	4.89	3.78				
20	3.23	3.19	3.18	3.24	3.52	3.27	3.84	3.66	3.08	2.79				
30	1.99	2.00	2.00	2.00	2.11	2.00	2.18	2.14	1.86	2.09		2.67	4.33	3.24
40	1.27	1.31	1.31	1.28	1.26	1.26	1.19	1.23	1.17	1.59		2.13	2.75	2.10
50	0.921	0.945	0.947	0.929	0.846	0.907	0.750	0.801	0.849	1.22		1.72	1.96	1.47
60	0.746	0.747	0.748	0.746	0.655	0.739	0.588	0.624	0.701	0.920		1.35	1.37	1.14
70	0.596	0.580	0.579	0.592	0.521	0.598	0.488	0.507	0.580	0.637		1.06	1.05	0.889
80	0.410	0.388	0.387	0.408	0.363	0.418	0.354	0.359	0.417	0.370		0.778	0.812	0.643
90	0.206	0.189	0.188	0.207	0.185	0.216	0.191	0.188	0.224	0.150		0.419	0.604	0.400
100	0.054	0.045	0.045	0.054	0.051	0.060	0.060	0.056	0.061	0.032		0.156	0.384	0.168
110	0.031	0.028	0.027	0.020	0.031	0.032	0.037	0.034	0.0031	0.059		0.0291	0.211	0.035
120	0.190	0.184	0.184	0.159	0.174	0.188	0.173	0.174	0.108	0.252		0.0217	0.0404	0.0536
130	0.539	0.521	0.519	0.479	0.488	0.537	0.477	0.483	0.393	0.596		0.229	0.0651	0.0268
140	1.03	0.994	0.991	0.942	0.935	1.04	0.913	0.925	0.821	1.04		0.636	0.260	0.643
150	1.59	1.52	1.52	1.47	1.44	1.60	1.40	1.42	1.32	1.52		1.18	0.657	1.10
160	2.10	2.01	2.00	1.95	1.89	2.11	1.85	1.88	1.78	1.94		1.87	1.17	1.31
170	2.45	2.34	2.33	2.28	2.21	2.47	2.17	2.19	2.10	2.23			1.74	
l						Partial-wave contribution to $\sigma_{abs}(a_0^2)$								
0	0.084	0.110	0.112	0.158	0.152	0.088	0.157	0.154	0.501	0.046				
1–5	1.725	1.729	1.726	1.644	3.000	1.731	4.121	3.508	1.348	1.211				
6–10	0.037	0.010	0.011	0.040	0.055	0.031	0.130	0.087	0.002	0.597				
11–15	5.0(−3)	4.3(−5)	2.0(−5)	7.5(−4)	9.6(−5)	5.3(−5)	2.3(−4)	1.5(−4)	2.6(−6)	0.224				
16–∞	0	0	0	0	0	0	0	0	0	0.261				

[a]Reference 17.
[b]Reference 24.
[c]Reference 22.
[d]Reference 18.

the absorption cross sections all shift in the same order. We performed an additional calculation in which we used the version 3 potential for $r \leq 2.0a_0$ and joined it smoothly to the original quasifree-scattering model potential for $r \geq 2.4a_0$; this yielded $\sigma_{abs} = 3.51a_0^2$, indicating that about half the increase in σ_{abs} in changing the quasifree absorption potential from the original version to version 3 comes from the vicinity of the minimum $(r \lesssim 2.2a_0)$, and the other half comes from large r $(r \gtrsim 2.2a_0)$.

IV. QUASIFREE-SCATTERING MODEL, VERSION 3

Tests for He, Ne, and Ar show that the quasifree-scattering model, version 3, gives systematically better large-angle differential cross sections than any other ver-
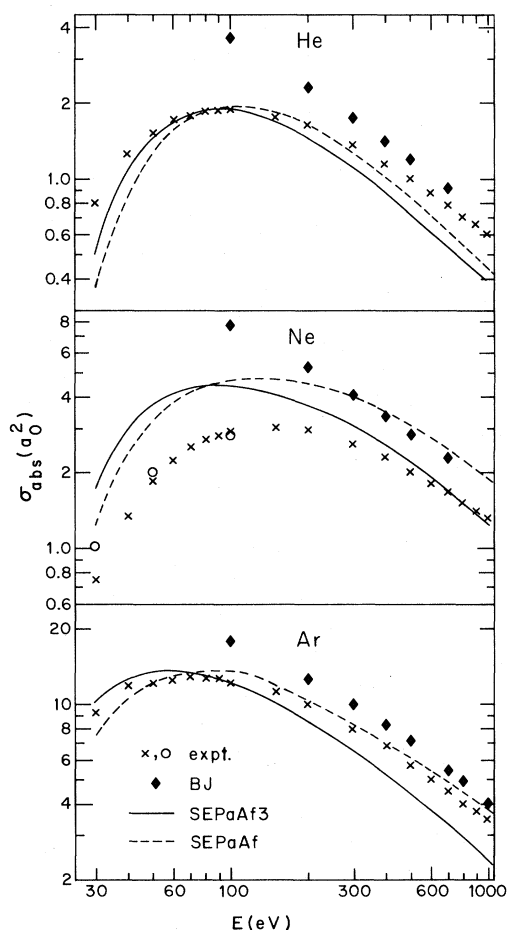
FIG. 6. Absorption cross sections as a function of energy for electron scattering by He, Ne, and Ar: ———, quasifree-scattering model, version 3; – – –, original quasifree-scattering model; ◆, optical eikonal model (for He and Ne, these are obtained by integrating the elastic differential cross sections given in Ref. 9 and subtracting from the total scattering cross sections given in the same reference; for Ar, these are obtained by subtracting the elastic integral cross sections given in Ref. 10 from the total scattering cross sections given in the same reference); ✕, experiments by de Heer et al. (He, Ref. 16; Ne, and Ar, Ref 17); ○, experimental lower bounds by Register and Trajmar, Ref. 18.
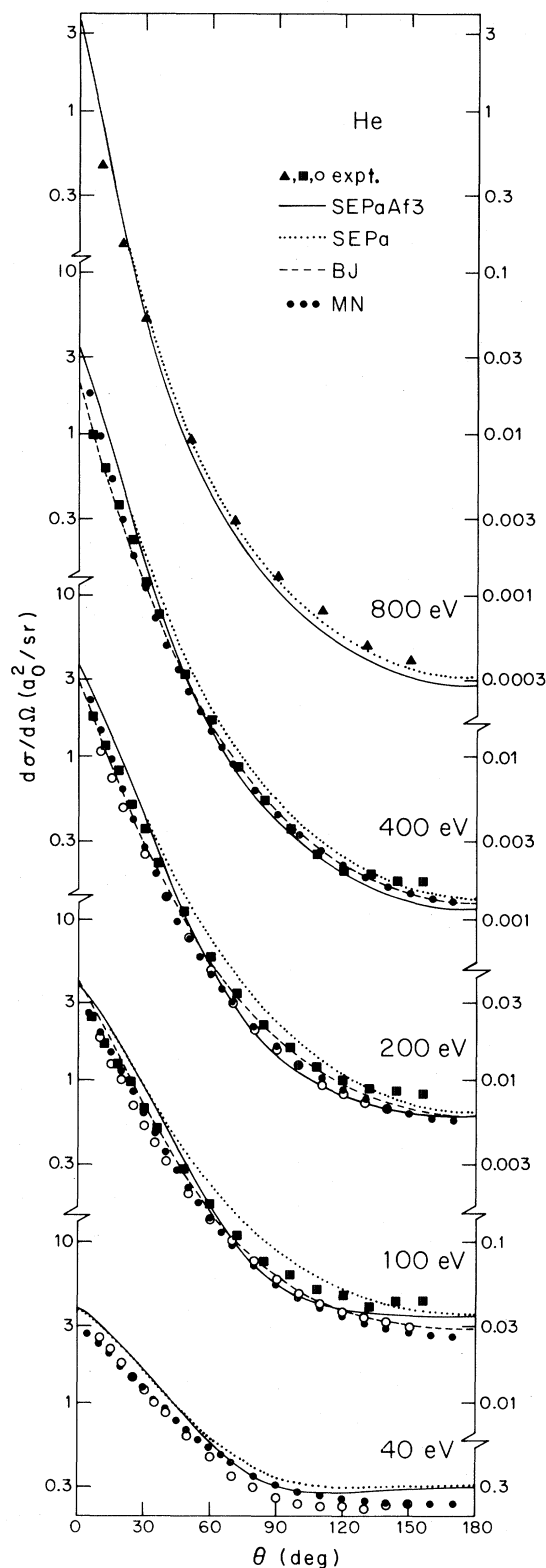
FIG. 7. Differential cross sections for electron scattering by He at 40-, 100-, 200-, 400-, and 800-eV impact energies: ———, quasifree-scattering model, version 3; · · · ·, SEPa model without absorption; – – –, calculations by Byron and Joachain, Ref. 9; ● ● ●, calculations by McCarthy, Noble, and co-workers, Ref. 2; ▲, experiments by Crooks, Ref. 19; ■, experiments by Shyn, Ref. 20; ○, experiment by Register et al., Ref. 21.
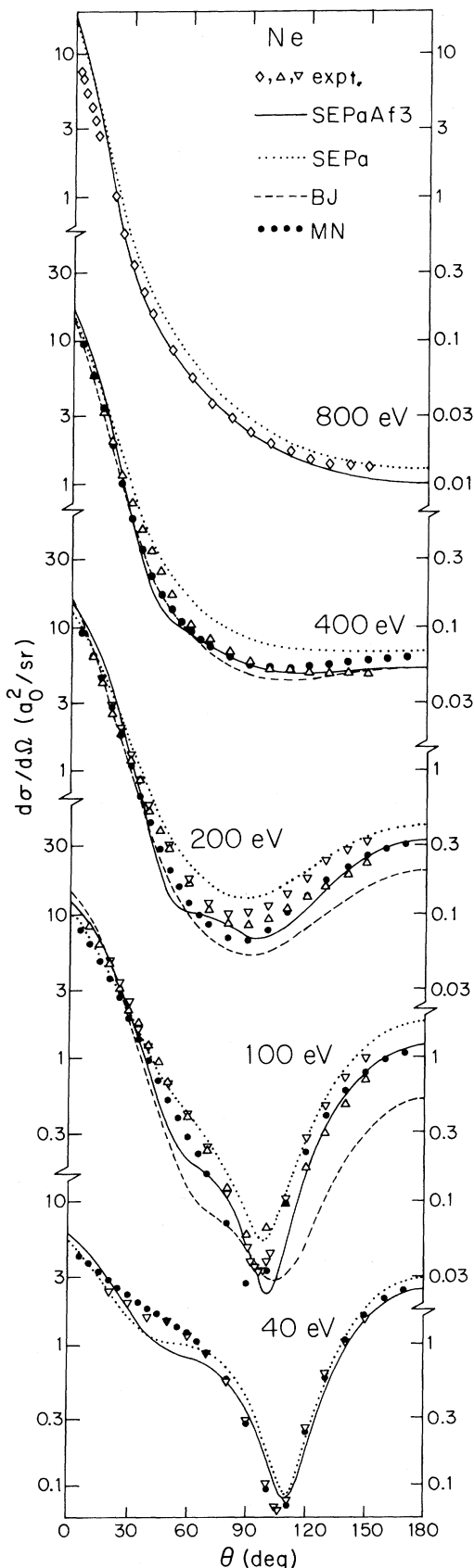
FIG. 8. Same as Fig. 7, except for electron scattering by Ne and the symbols denote: ◇, experiments by Dubois and Rudd, Ref. 22; △, experiments by Gupta and Rees, Ref. 23; ▽, experiments by Williams and Crowe, Ref. 24.

sion of the quasifree-scattering model. The predicted absorption cross sections for these three targets are illustrated in Fig. 6. The results are systematically better than the eikonal optical model. The quasifree-scattering model appears to overestimate the absorption cross sections for Ne, but the experimental results of Ref. 17 may be too low for Ne. Independent evidence for this is the fact that the experimental lower bounds of Ref. 18 exceed the results of Ref. 17 at 30 and 50 eV. It is also consistent that the eikonal optical model overestimates the absorption cross section for Ne much more than for the other two targets.

In comparison to the original version, the quasifree-scattering model version 3 gives more absorption for small energies and less for large energies. For He and Ar the maximum percentage error in the range of energies shown in Fig. 6 occurs for energy 1000 eV and is 36% for He and 30% for Ar. The main difference between this version of the quasifree-scattering model and the original one comes from the region close to the small-r cutoff of the potential. The new potential is weaker in this region, and the large-angle differential cross section is very sensitive to this region for higher energies.

Figures 7—9 show the differential cross sections of the quasifree-scattering model, version 3, for all three targets at a consistent set of energies. These results are compared to experiment, to the calculations of Byron and Joachain and McCarthy, Noble, and co-workers, and to the predictions obtained with no absorption potential. The figures show that without absorption the calculated differential cross sections are usually greater than the experimental ones. A primary motivation for introducing an absorption potential is to decrease this systematic error in the results obtained with a real potential. The agreement of the new model with experiment is generally successful at improving this situation, although for Ar at 400 eV the improvement in agreement of the theory with the large-angle experimental results of Williams and Willis[25] is less satisfactory than in other cases. Since we obtain better agreement with experiment at 200 and 800 eV for Ar, we attribute a large part of the disagreement with the experiment of Williams and Willis at 400 eV to experimental error. As a check on this conclusion, Fig. 10 shows a comparison to experiment at 500 eV for Ar. We obtain good agreement, and this gives further support to the conclusion that the experimental results for Ar at 400 eV are too low. It is consistent that the eikonal optical model and the model of McCarthy, Noble, and co-workers are also larger than experiment at this energy for Ar.

V. CONCLUSIONS

The goal of the present study was to investigate how the shape of absorption potential influences the absorption and differential cross sections. These cross sections are more sensitive to the choice of absorption potential at high energy than at intermediate energy, so we concentrated on understanding why some of the models are less accurate at higher energies. Our main conclusions are the following.

(i) The large-angle scattering is very sensitive to the small-r absorption potential. A too strong potential in
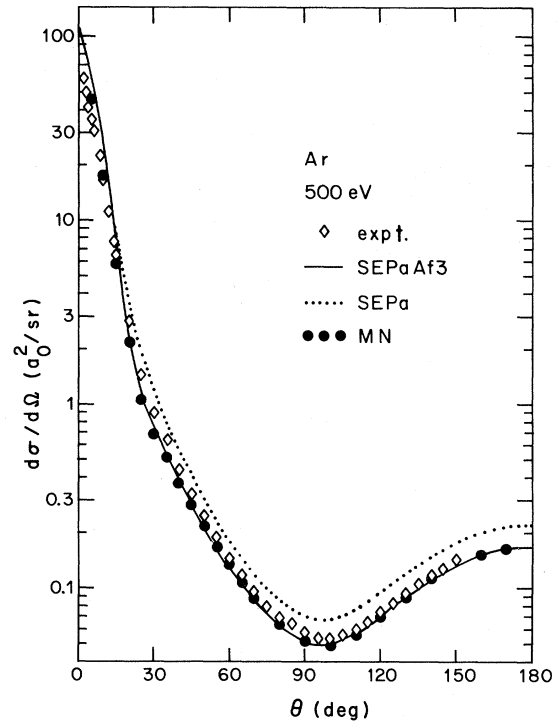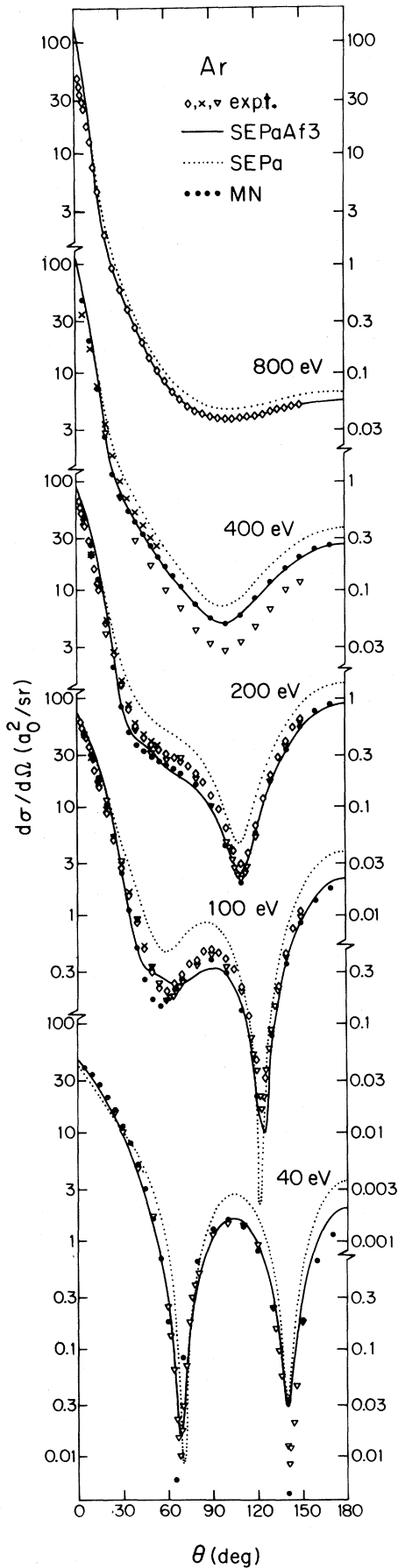
FIG. 10. Same as Fig. 9, except for 500 eV.

this region lowers the large-angle differential cross section considerably.

(ii) The long-range absorption potential has much less influence on the differential cross section but has a large effect on the absorption cross section.

(iii) It is rather unimportant how the absorption potential behaves very close to the origin.

According to these observations we modified the Pauli blocking in the quasifree-scattering model to get a weaker absorption potential for small r and a stronger one for large r. The new Pauli-blocking condition is explicitly dependent on the local increase in kinetic energy of the incident electron as caused by the static-exchange field of the target and produces larger changes for higher energies (where the absorption potential is stronger and where the original quasifree-scattering model is worse). The new Pauli-blocking condition depends only on features of target such as the ionization potential, the energy gap, and the static-exchange potential, so it is quite general, and it can be applied to any target without adjusting any parameters. The differential cross sections we obtained with the new model for He, Ne, and Ar are quite satisfactory. The absorption cross sections are a little worse than we obtained with the original quasifree-scattering model but still reasonable.

Equation (5) for the absorption potential is a general functional of the Pauli-blocking condition and is susceptible to various empirical modifications. Our version 3

FIG. 9. Same as Fig. 7, except for electron scattering by Ar and the symbols denote: ∇, experiments by Williams and Willis, Ref. 25; $\times$, experiments by Jansen et al., Ref. 26.

shows that one can get a big improvement over the original quasifree-scattering model even with a parameter-free Pauli-blocking function. Further improvement may be possible by introducing parameters, if desired. The major inaccuracy in version 3 for the three rare gases considered is that the absorption cross section is underestimated for higher energies. Apparently we need a longer-range absorption potential for these energies. For small energies the new absorption potential appears to be too strong only for Ne, and the quantitative evaluation for Ne is clouded by uncertainties in the accuracy of the experimental data.

ACKNOWLEDGMENTS

APPENDIX A: GLOSSARY OF ABBREVIATIONS

We use capital letters to denote calculations performed by others:

BJ   Byron and Joachain[9] or Joachain, Vanderpoorten, Winters, and Byron;[10]
MN   McCarthy, Noble, and co-workers.[2]

For calculations performed by us we use the notation SEPyAz where S, E, P, and A denote the inclusion of static, exchange, polarization, and absorption terms in the effective potential, and y and z are lower case abbreviations denoting the forms of the polarization and absorption terms. We consider two forms for the polarization potential:

a   adiabatic approximation;
lke   local-kinetic-energy semiclassical approximation.

We consider several models for the absorption potential:

cf   original quasifree-scattering model times an empirical scale factor, Eq. (20);
cρ   an empirical scale factor times the target density;
cρj   arbitrary modification j of the cρ model;
d(OT) dispersion-relation absorption potential based

on the energy-dependent polarization potential of Onda and Truhlar;
eo   eikonal optical model;
eoj   arbitrary modification j of the eo model;
f   original quasifree-scattering model;
f2   quasifree-scattering model, version 2, Eq. (21);
f3   quasifree-scattering model, version 3, Eq. (22);
G   model of Green et al.;[3]
mf   model of Furness and McCarthy,[1] Eqs. (15) and (16);
mn   model of McCarthy, Noble, and co-workers,[2] Eqs. (16) and (17);
m3   model of the type used by McCarthy and co-workers, version 3, Eqs. (16) and (18).

We also consider the SEPa model, which neglects absorption.

APPENDIX B: CALCULATIONAL DETAILS

The calculational details for everything except the absorption potentials are the same as for previously published work[4,5,12−15,28−30] and are summarized in this appendix.

The static potentials and densities for He and Ne are taken from Strand and Bonham,[36] as discussed previously.[15] The static potentials and density for Ar are taken from our own ab initio extended-basis-set Hartree-Fock (EBSHF) calculations.[14] All exchange potentials are computed by the semiclassical exchange approximation.[32]

Adiabatic polarization potentials are spline fits to our group's ab initio EBSHF variational calculations, as presented elsewhere for He,[5] Ne,[37] and Ar.[14] The local-kinetic-energy semiclassical polarization approximation[38] for Ne was based on Eqs. (3) and (9) of Ref. 29. The gaps and ionization potentials are 19.82 and 24.48 eV, respectively, for He, 16.62 and 21.559 eV for Ne, and 11.55 and 15.755 eV for Ar.

The scattering calculations were carried out by our complex phase equation program.[5,28,30] All differential and absorption cross sections were carefully converged with respect to l_{max}, the maximum orbital angular momentum included in the sums.

The elastic differential, integral, and momentum-transfer cross sections are called $d\sigma_{el}/d\Omega$, σ_{el}, and σ_{el}^m, respectively. The absorption cross section is called σ_{abs}, and the total scattering cross section, which is the sum of σ_{el} and σ_{abs}, is called σ_{tot}.

*Permanent address: Institute of Physics, Nicholas Copernicus University, Toruń, Poland.

[1]J. B. Furness and I. E. McCarthy, J. Phys. B 6, 2280 (1973).

[2]I. E. McCarthy, C. J. Noble, B. A. Phillips, and A. D. Turnbull, Phys. Rev. A 15, 2173 (1977).

[3]A. E. S. Green, D. E. Rio, and T. Ueda, Phys. Rev. A 24, 3010 (1981).

[4]D. Thirumalai and D. G. Truhlar, Phys. Rev. A 26, 793 (1982); 28, 3140(E) (1983).

[5]D. Thirumalai, D. G. Truhlar, M. A. Brandt, R. A. Eades, and

D. A. Dixon, Phys. Rev. A 25, 2946 (1982).

[6]F. W. Byron, Jr., Phys. Rev. A 9, 2559 (1974).

[7]F. W. Byron, Jr. and C. J. Joachain, Phys. Lett. 49A, 306 (1974).

[8]R. Vanderpoorten, J. Phys. B 8, 926 (1975).

[9]F. W. Byron, Jr., and C. J. Joachain, Phys. Rev. A 15, 128 (1977).

[10]C. J. Joachain, R. Vanderpoorten, K. H. Winters, and F. W. Byron, Jr., J. Phys. B 10, 227 (1977).

[11]F. W. Byron, Jr. and C. J. Joachain, Phys. Rep. 34, 233

(1977).

[12]S. M. Valone, D. Thirumalai, and D. G. Truhlar, Int. J. Quantum Chem. Symp. 15, 341 (1981).

[13]G. Staszewska, D. W. Schwenke, D. Thirumalai, and D. G. Truhlar, J. Phys. B 16, L281 (1983).

[14]G. Staszewska, D. W. Schwenke, and D. G. Truhlar, Int. J. Quantum Chem. Symp. 17, 163 (1983). Errata: in Table II, 0.008 80 should be 0.0880, 0.000 559 should be 0.005 59, and 0.000 002 35 should be 0.000 023 5; in Table III, 31.6 should be 13.6, 21.0 should be 22.0, 8.79 sould be 8.78, and 25.07 should be 25.08.

[15]G. Staszewska, D. W. Schwenke, D. Thirumalai, and D. G. Truhlar, Phys. Rev. A 28, 2740 (1983).

[16]F. J. deHeer and R. H. J. Jansen, J. Phys. B 10, 3741 (1977).

[17]F. J. deHeer and R. H. J. Jansen, and W. van der Kaay, J. Phys. B 12, 979 (1979).

[18]D. F. Register and S. Trajmar, Phys. Rev. A 29, 1785 (1984).

[19]G. B. Crooks, Ph. D. thesis, University of Nebraska, 1972.

[20]T. W. Shyn, Phys. Rev. A 22, 916 (1980).

[21]D. F. Register, S. Trajmar, and S. K. Srivastava, Phys. Rev. A 21, 1134 (1980).

[22]D. R. Dubois and M. E. Rudd, J. Phys. B 9, 2657 (1976).

[23]S. C. Gupta and J. A. Rees, J. Phys. B 8, 417 (1975). The elastic momentum-transfer cross sections corresponding to this study are the recomputed values of Ref. 28.

[24]J. F. Williams and A. Crowe, J. Phys. B 8, 2233 (1975).

[25]J. F. Williams and B. A. Willis, J. Phys. B 8, 1670 (1975).

[26]R. H. J. Jansen, F. J. deHeer, H. J. Luyken, B. Van Wingerden, and H. J. Blaauw, J. Phys. B 9, 185 (1976).

[27]S. K. Srivastava, H. Tanaka, A. Chutjian, and S. Trajmar, Phys. Rev. A 23, 2156 (1981).

[28]D. Thirumalai and D. G. Truhlar, Phys. Rev. A 25, 3058 (1982).

[29]D. Thirumalai and D. G. Truhlar, Phys. Rev. A 27, 158 (1983).

[30]G. Staszewska, D. W. Schwenke, and D. G. Truhlar, Phys. Rev. A 28, 169 (1983).

[31]D. G. Truhlar, in *Chemical Applications of Atomic and Molecular Electrostatic Potentials,* edited by P. Politzer and D. G. Truhlar (Plenum, New York, 1981), p. 123.

[32]M. E. Riley and D. G. Truhlar, J. Chem. Phys. 63, 2182 (1975).

[33]D. G. Truhlar, D. A. Dixon, R. A. Eades, F. A. Van-Catledge, and K. Onda, in *Electron-Molecule and Photon-Molecule Collisions,* edited by T. N. Rescigno, V. McKoy, and B. I. Schneider (Plenum, New York, 1979), p. 151.

[34]R. Lipperheide, Z. Phys. 202, 508 (1967).

[35]K. Onda, and D. G. Truhlar, Phys. Rev. A 22, 86 (1980).

[36]T. G. Strand and R. A. Bonham, J. Chem. Phys. 40, 1686 (1964).

[37]C. H. Douglass, Jr., D. A. Weil, P. A. Charlier, R. A. Eades, D. G. Truhlar, and D. A. Dixon, in *Chemical Applications of Atomic and Molecular Electrostatic Potentials,* edited by P. Politzer and D. G. Truhlar (Plenum, New York, 1981), p. 173.

[38]S. M. Valone, D. G. Truhlar, and D. Thirumalai, Phys. Rev. A 25, 3003 (1982).